NUKLEONIKA 2013;58(3):347–350

ORIGINAL PAPER

Modelling of EMR data for $Fe^{2+}(S=2)$ ions in a [2Fe-2S] cluster in the reduced ferredoxin

Czesław Rudowicz, Danuta Piwowarska, Paweł Gnutek

Abstract. The modelling techniques employed in this study utilize structural data to enable correlation of EMR data – described by the spin Hamiltonian (SH) and optical spectroscopy data – described by the crystal field (CF) Hamiltonian. These techniques enable also to predict magnetic and spectroscopic properties of $3d^N$ ions, especially $3d^4$ and $3d^6$ ions, in various systems. Specific applications are considered for [Fe^{2+} and Fe^{3+}] binuclear centres in [2Fe-2S] cluster in the reduced ferredoxin and related biological molecules. The background for model calculations of the zero-field splitting (ZFS) parameters and/or crystal field parameters and the capabilities of the two major techniques used will be presented in the full paper. Here, we present preliminary results of the microscopic spin Hamiltonian (MSH) modelling for Fe^{2+} ($3d^6$) ions in the reduced ferredoxin.

Key words: [2Fe-2S] cluster • electron magnetic resonance (EMR) • Fe^{2+} ions • microscopic spin Hamiltonian (MSH) • zero field splitting (ZFS) parameters

C. Rudowicz✉, D. Piwowarska, P. Gnutek
Institute of Physics,
West Pomeranian University of Technology,
17 Piastów Ave., 70-310 Szczecin, Poland,
Tel.: +48 91 449 4585, Fax: +48 91 449 4181,
E-mail: crudowicz@zut.edu.pl

Received: 17 September 2012
Accepted: 19 December 2012

Introduction

Iron-sulphur (Fe-S) proteins are functional in many biological processes where they act as electron carriers [5]. The properties and functions of iron-sulphur clusters in Fe-S proteins have recently been surveyed in [1]. Several classes of such clusters were identified in Fe-S proteins, including [2Fe-2S], [3Fe-4S], and [4Fe-4S], where the iron ions are tetrahedrally coordinated with bridging sulphide ions and generally ligated by cysteinyl residues [1, 2, 7]. Although ferredoxin-type [2Fe-2S] clusters with four cysteine ligands are most common, another type of such cluster, named Rieske-type, has histidine ligands replacing two of the cysteines near one of the iron atoms. This cluster exhibits spectral and chemical properties that distinguish it from the [2Fe-2S] cluster of plant ferredoxins [13]. Strong antiferromagnetic coupling between the electronic spins of the two iron ions via a bridging structure produces an electron magnetic resonance (EMR)-silent ground state ($S = 0$) in the oxidized Fe^{3+}-Fe^{3+} form of the cluster, whereas a paramagnetic ground state ($S = 1/2$) in the reduced Fe^{3+}-Fe^{2+} form [20].

The present study focuses on modelling the magnetic and spectroscopic properties of [Fe^{2+} and Fe^{3+}] binuclear centres in [2Fe-2S] cluster in the reduced ferredoxin and related biological molecules. The modelling techniques utilize structural data to enable correlation of EMR data – described by the spin Hamiltonian (SH) and optical spectroscopy data – described by the crystal field (CF) Hamiltonian. The background for superposition model calculations of the zero-field splitting (ZFS) parameters and/or crystal field (CF)

parameters has been presented in [16]. Two major techniques employed are: (i) the package MSH/VBA [18] developed in Visual Basic in Application (VBA) in Excel environment based on the microscopic spin Hamiltonian (MSH) theory, which includes also graphical capabilities and is especially useful for the $3d^4$ and $3d^6$ ($S = 2$) ions at tetragonal, trigonal, and orthorhombic symmetry sites [19] and (ii) the CF analysis (CFA) package [11] which is suitable for the $3d^N$ ions at arbitrary symmetry sites in crystals, and includes the MSH module for axial symmetry cases. Preliminary microscopic modelling results for the $Fe^{2+}(3d^6)$ ions with spin $S = 2$ in the reduced forms of rubredoxin (Rd_{red}) are presented here. Illustrative examples of potential applications of these techniques for other $3d^4$ and $3d^6$ ($S = 2$) ions in biological systems will be discussed in the full paper together with a comparative analysis of our results with the pertinent ones obtained using density functional theory (DFT) techniques [10, 21].

Theoretical background

Iron-sulphur [2Fe-2S] proteins are characterized by the presence of polymetallic systems containing sulphide ions, in which the iron ions have variable oxidation states. The simplest polymetallic system is constituted by two iron ions bridged by two sulphide ions, coordinated by four cysteinyl ligands in Fe_2S_2 ferredoxins [4] or by two cysteines and two histidines in Rieske proteins [9, 14]. The oxidized proteins contain two Fe^{3+} ions, whereas the reduced proteins contain one Fe^{3+} and one Fe^{2+} ion. For illustration, we present the data for typical structures of iron-sulphur [2Fe-2S] proteins taken from the Protein Data Bank (PDB) [3]: (a) soluble C-terminal fragments of Rieske proteins from bovine heart mitochondrial cytochrome bc_1 complex (PDB [3] ID: 1RIE [12] – monoclinic space group $P2_1$ (No. 4) with $a = 3.21$ nm, $b = 5.30$ nm, $c = 3.80$ nm and $\beta = 100.3°$) and (b) spinach chloroplast cytochrome b_6f complex (PDB [3] ID: 1RFS [8] – triclinic space group $P1$ (No. 1) with $a = 2.905$ nm, $b = 3.187$ nm, $c = 3.579$ nm, $\alpha = 95.6°$, $\beta = 106.1°$ and $\gamma = 117.3°$). In both the [2Fe-2S] clusters the two iron ions are located at triclinic symmetry sites.

In the oxidized Fe^{3+}-Fe^{3+} form of the [2Fe-2S] cluster the strong antiferromagnetic interactions between the electron spins of two irons via a bridging structure produce the ground state with $S = 0$, whereas in the reduced form $Fe^{3+}(S = 5/2)$-$Fe^{2+}(S = 2)$, a paramagnetic $S = 1/2$ ground state. Thus, the reduced form of the [2Fe-2S] cluster in frozen solutions is characterized by the anisotropic EPR spectrum typically as a result of a rhombic g-tensor [20]. Note that the g-tensor used in [20] should be considered as expressed in the principal axis system. Detailed analysis of the axis systems will be presented in the full paper.

Transitions between the CF levels are in the realm of optical spectroscopy, whereas transitions within the spin states of the ground orbital singlet – in the realm of EMR. Theoretical basis of the MSH analysis used for interpretation of the experimental data for Fe^{2+} ions and hence the [2Fe-2S] cluster may be found in [5, 6, 15, 18]. The effective total g-tensor for the ground state of the [2Fe-2S] cluster is determined by the relation [4, 5, 10, 20, 21].

$$\mathbf{g} = \frac{7}{3}\mathbf{g}_1(Fe^{3+}) - \frac{4}{3}\mathbf{g}_2(Fe^{2+}) \quad (1)$$

Both Fe^{3+} and Fe^{2+} ions in [2Fe-2S] clusters have a distorted tetrahedral coordination. As a first approximation, the coincident principal directions of g_1 and g_2 are assumed [20]. Then, the environment of Fe^{2+} ion in Rieske-type [2Fe-2S] clusters is often approximated by the C_{2v} distorted tetrahedral coordination with two histidine and two cysteines ligands. Spectroscopic properties of the $3d^N$ ions in crystals are determined by the CF energy levels and states. The energy levels scheme of the Fe^{2+} ions in Rd_{red} systems correspond to the energy levels $\{\Delta_i\}$ scheme denoted αOII1 in the package MSH/VBA [18, 19] with Δ_1, Δ_2, Δ_3 corresponding to Δ_{yz}, Δ_{xz}, Δ_{xy} in [20], respectively. Additionally, the correlation of the wave functions yields the mixing coefficient θ used in [18, 19] corresponding to $(\pi/2 - \theta)$ in [20]. Detailed analysis of the energy levels, wave functions, and mixing coefficients will be presented in the full paper.

Results and discussion

Selected sets of model parameters

The energy levels and mixing coefficient (s) adopted from Ref. [20] for calculations of the Zeeman g_i factors and the ZFS parameters [18, 19] are listed in Table 1. Shubin and Dikanov in their Table 1 [20] have provided the minimum and maximum values of the mixing angle θ for each set of parameters obtained during the fitting of the experimental g-tensors for the [2Fe-2S] cluster. The intervals $(\theta_{max} - \theta_{min})$ are rather small and vary slightly for their sets I to III, which were considered as most reasonable, whereas are larger and vary significantly for their sets IV to VII, which were considered as deficient in some respects by some authors [20]. In order to reduce the modelling calculations to a manageable number of input datasets, we have selected only the energy levels Δ_{ij} given in their sets I to III and denoted them as sets 1 to 3 in our Table 1, respectively. For the same reason, we have adopted the average values of the mixing angles $\theta_{av} = (\theta_{max} + \theta_{min})/2$, as listed in Table 1, and recalculated them for the mixing coefficients $s_{av} = \sin(\pi/2 - \theta_{av})$ [18, 19]. In order to consider variations of the spin Hamiltonian parameters with the microscopic

Table 1. The selected sets of parameters of the energy levels Δ_{ij} (in cm^{-1}) for Fe^{2+}: [2Fe-2S] adopted from [20] for calculations of the spin Hamiltonian parameters

Set	$\Delta_{yz} \equiv \Delta_1$	$\Delta_{xz} \equiv \Delta_2$	$\Delta_{xy} \equiv \Delta_3$	Δ_4	s_{av}	θ_{av}
1	1900	15 000	650	15 500	0.8842	–27.85
2	2497	30 526	640	31 026	0.8961	–26.35
3	616	18 090	347	18 590	0.7296	–43.15

Table 2. The calculated Zeeman factors ($i = x, y, z$) for Fe^{2+}:[2Fe-2S]: g_{2i} – contributions due only to the second-order spin-orbit coupling, g_{2iT} – the total values, and the relative percentage differences Δg_{2i} defined in text; $g_e = 2.0023$

Set	$g_{2i} = g_e + \Delta g_{2i}(\lambda)$			g_{2iT}			Δg_{2i} (%)			
	g_{2x}	g_{2y}	g_{2z}	g_{2xT}	g_{2yT}	g_{2zT}	Δg_{2x}	Δg_{2y}	Δg_{2z}	$\Delta\bar{g}_{2i}$
1	2.0977	2.0449	2.2172	2.0421	1.9766	2.1601	2.7	3.3	2.6	2.9
2	2.0810	2.0232	2.1993	2.0309	1.9640	2.1484	2.4	2.9	2.3	2.6
3	2.0896	2.0358	2.8650	1.6942	1.5875	2.4654	18.9	22.0	14.0	18.3

Table 3. The total ZFS parameters b_k^q for Fe^{2+}:[2Fe-2S]

Set	b_2^0	b_2^2	b_4^0	b_4^2	b_4^4
1*A*i	–5.4991	–4.0243	0.0997	0.4763	0.2848
2*A*i	–5.4769	–3.9335	0.1065	0.3309	0.1775
3*A*i	–19.3300	–8.7285	5.9851	6.5630	1.1052

ones, the following variants of parameter sets are included in our calculations (in cm^{-1}): (*A*) with $\lambda = -80$, $\rho_A = 0.18$ and differing by Δ_4: (*A*i) $\Delta_4 \equiv$ Max + 500 and (*A*ii) $\Delta_4 \equiv$ Max + 1000, and (*B*) differing by ρ: (*B*i) and (*B*ii) with $\rho_B = 1.00$ and other respective parameters as in sets (*A*i) and (*A*ii), respectively. By 'Max' we denote the available maximum energy of the third excited state for a given set.

Calculated spin Hamiltonian parameters

In order to visualize the role of the additional contributions to the Zeeman g_i factors included in the extended perturbation expressions [18, 19] g_{2iT} with respect to the second-order spin-orbit coupling contributions, g_{2i}, only included by other authors [5, 20] the relative percentage differences are defined as follows

$$\Delta g_{2i} = \frac{|g_{2iT} - g_{2i}|}{g_{2i}} \cdot 100\% \tag{2}$$

Our calculations reveal that for all variants, the relative percentage differences Δg_{2i} are around 3% for the set 1 and 2, whereas around 19% for the set 3 (Table 2).

The total standardized [15–17] ZFS parameters for Fe^{2+} in the [2Fe-2S] proteins for the variant *A*i are presented in Table 3. Note that the calculated ZFS parameters for the sets 1 to 3 from Table 1 are standard and nearly the same for the variants *A*i (*B*i) and *A*ii (*B*ii), thus showing that these quantities depend only slightly on the variables Δ_4 and ρ [18]. Hence, we refrain from presenting the results for the type (ii) variants.

For illustration, the variations of the total second-rank ZFS parameters b_2^0 and b_2^2 for Fe^{2+}:[2Fe-2S] with the spin-orbit coupling constant λ for the sets 1 to 3 from Table 3 and using the variant *A* with $\rho_A = 0.18$ cm^{-1} are presented in Fig. 1. The variations of the fourth-rank ZFS parameters b_4^q have also been considered and will be presented in the full paper.

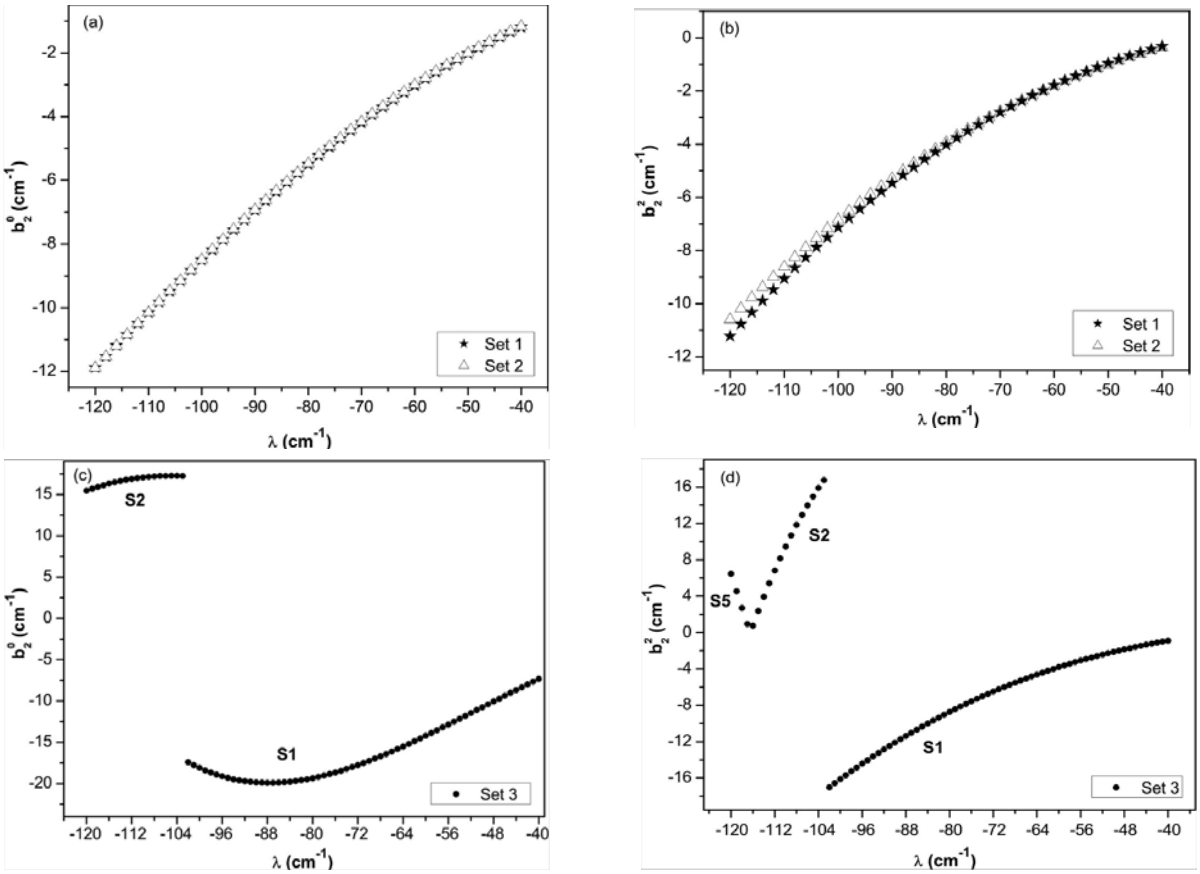

Fig. 1. Variation of the total second-rank ZFS parameters b_2^0 and b_2^2 for Fe^{2+}:[2Fe-2S] with λ for the sets 1 to 3 (Table 1) and the variant *A* ($\rho_A = 0.18$ cm^{-1}).

It is seen in Figs. 1a and 1b that for the set 1 and 2, the value of $|b_2^0|$ and $|b_2^2|$ decrease while the absolute value of $|\lambda|$ decreases and remain standard [15–17] in the range of λ considered. For the set 3, some peculiarities are observed, which arise due to orthorhombic standardization since the package MSH/VBA [18, 19] transforms automatically the ZFS parameters from a non-standard region to the standard region $S1$ [15–17]. Overall after standardization the values of b_2^q are positive for λ in the range (–120, –102) cm^{-1} and negative for λ α (–102, –40) cm^{-1} (Figs. 1c and 1d). However, the non-standardized parameter b_2^2 changes the sign first at about $\lambda = -117\ cm^{-1}$ due to the transformation from the $S5$ to $S2$ region, whereas the apparent jumps for the set 3 at about $\lambda = -102\ cm^{-1}$ are due to the transformation from the $S2$ to $S1$ region. The results for several other data sets and their detailed analysis will be presented in the full paper.

Conclusions

The capabilities of the modelling technique, i.e. the package MSH/VBA based on microscopic spin Hamiltonian (MSH) theory, have been demonstrated using as a case study model calculations of the spin Hamiltonian parameters for Fe^{2+} ions in the reduced ferredoxin. The preliminary results for the Zeeman g_i factors and the second-rank zero field splitting (ZFS) parameters are presented here. The variation of the total second--rank ZFS parameters b_2^2 and b_2^2 for Fe^{2+} in the [2Fe-2S] cluster with the spin-orbit coupling constant λ reveals that for certain parameter sets obtained by Shubin and Dikanov [20] intricate aspects related to orthorhombic standardization must be considered. Detailed analysis of the extended results will be presented in the full paper. Our comparative analysis will enable bridging the gap between DFT and crystal-field based techniques for modelling of EMR and optical spectroscopic data.

References

1. Beinert H (2000) Iron-sulfur proteins: ancient structures, still full of surprises. J Biol Inorg Chem 5:2–15
2. Beinert H, Holm RH, Münck E (1997) Iron-sulfur clusters: Nature's modular, multipurpose structures. Science 277:653–659
3. Berman HM, Westbrook J, Feng Z *et al*. (2000) The Protein Data Bank. Nucleic Acids Res 28:235–242, http://www.pdb.org
4. Bertini I, Ciurli S, Luchinat C (1995) The electronic structure of FeS centers in proteins and models. A contribution to the understanding of their electron transfer properties. Struct Bond 83:1–53
5. Bertrand P, Gayda J-P (1979) A theoretical interpretation of the variations of some physical parameters within the [2Fe-2S] ferredoxin group. Biochim Biophys Acta 579:107–121
6. Bertrand P, Guigliarelli B, Gayda J-P, Peter B, Gibson JF (1985) A ligand-field model to describe a new class of 2Fe-2S clusters in proteins and their synthetic analogues. Biochim Biophys Acta 831:261–266
7. Cammack R (1992) Iron-sulfur clusters in enzymes: themes and variations. Adv Inorg Chem 38:281–322
8. Carrell CJ, Zhang H, Cramer WA, Smith JL (1997) Biological identity and diversity in photosynthesis and respiration: Structure of the lumenside domain of the chloroplast Rieske protein. Structure 5:1613–1625
9. Cowan JA (1993) Inorganic biochemistry: An introduction. VCH Publishers, New York
10. Gambarelli S, Mouesca J-M (2004) Correlation between the magnetic *g*-tensors and the local cysteine geometries for a series of reduced [2Fe-2S*] protein clusters. A quantum chemical density functional theory and structural analysis. Inorg Chem 43:1441–1451
11. Gnutek P, Yang Z-Y, Rudowicz C (2009) Modeling local structure using crystal field and spin Hamiltonian parameters: the tetragonal Fe_K^{3+}-O_I^{2-} defect center in $KTaO_3$ crystal. J Phys: Condens Matter 21:455402
12. Iwata S, Saynovits M, Link TA, Michel H (1996) Structure of a water soluble fragment of the 'Rieske' iron-sulfur protein of the bovine heart mitochondrial cytochrome bc1 complex determined by MAD phasing at 1.5 Å resolution. Structure 4:567–579
13. Link TA (1999) The structures of Rieske and Rieske-type proteins. Adv Inorg Chem 47:83–157
14. Mason JR, Cammack R (1992) The electron transport proteins of hydroxylating bacterial dioxygenases. Annu Rev Microbiol 46:277–305
15. Rudowicz C (1987) Concept of spin Hamiltonian, forms of zero field splitting and electronic Zeeman Hamiltonians and relations between parameters used in EPR. A critical review. Magn Reson Rev 13:1–89
16. Rudowicz C, Gnutek P (2009) Modeling techniques for analysis and interpretation of electron magnetic resonance (EMR) data for transition ions at low symmetry sites in crystals. A primer for experimentalists. Physica B 404:3582–3593
17. Rudowicz C, Qin J (2004) Can the low symmetry crystal (ligand) field parameters be considered compatible and reliable? J Lumin 110:39–64
18. Rudowicz C, Sung HWF (2003) Comparative analysis of the microscopic spin-Hamiltonian expressions used for the non-Kramers $Fe^{2+}(3d^6)$ ions with spin S=2 in reduced rubredoxin, desulforedoxin, and related systems. Physica B 337:204–220
19. Rudowicz C, Zhou Y-Y (1997) Computer package for microscopic spin Hamiltonian analysis of the $3d^4$ and $3d^6$ (spin $S = 2$) ions at orthorhombic and tetragonal symmetry sites. Comput Chem 21:45–50
20. Shubin AA, Dikanov SA (2006) Variations of *g*-tensor principal values in reduced [2Fe-2S] cluster of iron-sulfur proteins. Appl Magn Reson 30:399–416
21. Vrajmasu VV, Bominaar EL, Meyer J, Münck E (2002) Mössbauer study of reduced rubredoxin as purified and in whole cells. Structural correlation analysis of spin Hamiltonian parameters. Inorg Chem 41:6358–6371